Computational Modeling for Scanning Tunneling Microscopy of Physisorbed Molecules via Ab Initio Quantum Chemistry

Joseph Crystal, Linda Yu Zhang,† Richard A. Friesner,* and George W. Flynn

Department of Chemistry, Columbia University, New York, New York 10027

Received: July 10, 2001; In Final Form: November 26, 2001

Scanning tunneling microscopy images of molecular adsorbates on a graphite surface are modeled using the techniques of electron transfer theory. The results are compared with experimentally determined tunneling probabilities and are shown to be qualitatively (and to some extent quantitatively) in accord with the experimental data. The results provide new insight into the various factors that contribute to the features in STM images of molecular adsorbates.

I. Introduction

Over the past decade, scanning tunneling microscopy (STM) has rapidly become a powerful tool in the study of surfaces and their properties. More recently, STM has been utilized to investigate the self-assembly of molecules on surfaces, and the information obtained through these studies suggests that this technique will prove to be a useful resource in the development of electronic and optical devices on a molecular level. In light of the prevalent use of STM at the forefront of current research, a theoretical understanding of the tunneling mechanism involved has become all the more important.

A number of theoretical approaches have been developed for modeling the STM tunneling mechanism. Tersoff and Hamann concluded that STM provides a contour map of the local density of states (LDOS) at the Fermi level of the surface at the position of the tip.[1,2] Lang and co-workers later suggested that this surface image is modified in the presence of an adsorbate due to the contribution of the adsorbate to the LDOS at the Fermi level.[3] A more sophisticated modification of the same basic approach was later taken by Marcus et al. whereby some of the approximations made in previous work were eliminated.[4] A similar approach used by Whangbo et al. indicated the sensitivity of STM images to tip−surface interactions.[5] Dabrowski et al. were able to ascertain the correct reconstruction on a silicon surface using ab initio electronic structure calculations and modeling the STM image using the approach of Tersoff and Hamann.[6] Goddard and co-workers have proposed a new perturbative approach, with some promising results, to model the tunneling mechanism.[7] More recently, Corbel et al. combined ab initio calculations with a scattering formalism in order to model the STM images of pure copper surfaces.[8]

In the current study we make use of ab initio quantum chemical computational techniques, available for the calculation of electron-transfer matrix elements, to model the tunneling current in STM. A prior study by Coley et al.[9] indicated that quantum chemical techniques could be utilized to understand the STM images of MoS_2 and $MoTe_2$. In the current study we examine the feasibility of utilizing this technique for a graphite surface in the presence of adsorbed molecules. The justification for the application of this technique to the modeling of STM images is presented below.

Before discussing the computational methodology, several preliminary points need to be made. Our calculations involve the computation of the transfer matrix element between an electron localized on the tip in the ground state of the tip−sample complex and the ground state of the complex with the electron localized on the sample. Although for the calculated bias voltage there is most likely some contribution to the transfer matrix element from the excited states of the complex, no other energy states were included in the present study. The contribution of the excited states to the transfer matrix element will be examined in future studies.

A comparison of our results with experimental images shows that this technique provides reasonable qualitative agreement with experiment. Following the initial comparison a model is developed that allows a more quantitative comparison between the calculated matrix elements and the experimental images. The overall method offers new insight into the relationship between the geometry and electronic structure of adsorbates and their corresponding STM images.

II. Methodology

A. Analysis of the Approximations Inherent in the Use of a Localized Cluster Calculation to Model the Tunneling Current in an STM Experiment. The problem of computing the tunneling current in an STM experiment is similar, but not identical, to the calculation of the electron transfer rate between a donor and acceptor molecule in a condensed phase, such as liquid solution. The principal difference between the two calculations is the presence of electronic continua for both the tip and the sample in case of the STM; both systems also possess a continuum of vibrational states that must be taken into account if the absolute value of the current or electron transfer rate is to be computed. Our approach is based on an extension of the standard Marcus theory of electron transfer between molecules, which in turn is based on the Golden Rule expression for the dynamics of electron transfer as obtained from time dependent perturbation theory. This extension becomes quite complicated if absolute rate constants are desired, due to the necessity of taking into account the effects of the electronic continua upon the coupling matrix elements and the energy matching criteria. However, if one is only interested in the relative rates as a function of the position of the donor molecule (the tip) relative to the acceptor molecule (the surface−adsorbate), plausible simplifying approximations can be made which reduce the problem to a cluster calculation of the coupling matrix element between charge localized diabatic states. A derivation of this approximation is provided below. It should be noted that the

* Corresponding author.
† Current Address: Chemistry Department, Rutgers University.

10.1021/jp012629+ CCC: $22.00
Published on Web 02/12/2002

approximations are heuristic in character and that a rigorous evaluation of their quantitative validity is not attempted in this paper. Nevertheless, it will be explained why the approximations are expected to be qualitatively reasonable in modeling STM images.

In what follows, for the sake of simplicity, the analysis is carried out using electrons in noninteracting single particle orbitals. The use of single particle eigenstates makes it possible to decouple the dependence of the current on the relative position of the tip and sample from the remainder of the expression for the absolute rate of electron transfer. Our belief is that any qualitative conclusions would be unchanged in a full many body context. This is, however, a more complicated argument and will be pursued in another publication.

We consider the platinum tip plus its originating electrode as one subsystem, the donor, which we will refer to as the tip (t), and the adsorbed molecule plus the graphite electrode as a second subsystem, the acceptor, which we refer to as the sample (s). We want to use time dependent perturbation theory to compute the rate of transfer of an electron from the tip to the sample (or vice versa). A rigorous calculation along these lines would involve integrating over all thermally occupied states of the tip (t) and over the corresponding target states of the sample (s) to yield the final result for the transition rate:

$$P_{t\rightarrow s} = \frac{2\pi}{\eta}\sum_{k}\sum_{k'}\int |T_{kk'}|^2 g_{kk'}(E)\rho_k(E)\rho_{k'}(E)\,dE \qquad (1)$$

The states k and k′ represent one particle eigenstates on the tip and sample, respectively; the sum is over all occupied states of the tip and all unoccupied states of the sample. $T_{kk'}$ is the coupling matrix element between the charge localized diabatic states represented by k and k′ (i.e., the electron to be transported is initially occupying k and is then transferred to k′). The quantities $\rho_k(E)$ and $\rho_{k'}(E)$ are the density of vibrational states on the tip and sample, respectively, and the factor $g_{kk'}(E)$ is the vibrational coupling of the two states at energy E. Thus we include not only the electronic continua on the tip and sample (represented by the sums over k and k′) but also the vibrational continua associated with each electronic manifold. The variable E is taken to incorporate shifts in the relative energies of the two manifolds due to factors such as the biasing voltage; the details of these shifts are unimportant for our argument. The precise forms of ρ and g will also not be important for the computation of relative transition rates as a function of tip position, assuming that the only change upon displacement of the tip relative to the sample is in the electronic coupling matrix element—a physically reasonable assumption. In principle one could use eq 1 to evaluate the absolute value of the tunneling current. Because we will not be carrying out such an explicit evaluation, we define the quantity

$$f_{kk'}(E) = g_{kk'}(E)\rho_k(E)\rho_{k'}(E) \qquad (2)$$

in order to simplify the notation in what follows.

A brute force evaluation of eq 1 would involve the determination of the eigenstates of the tip and sample as well as the coupling matrix elements between these eigenstates. For very simplified models of the electronic structure of the tip and sample, such a calculation is feasible, at least in principle. However, if one wants to use a more realistic representation of the electronic wave functions (and such a representation is certainly necessary in the determination of contrast ratios that are observed in experiments of the type we are considering in this paper), enumeration of all of the relevant many particle eigenstates of both systems, as well as their couplings, is out of the question. We would therefore like to develop a formalism utilizing a cluster representation of the interacting D−A system (which can be effectively treated by standard ab initio quantum chemical methods for determining electronic coupling matrix elements) in which the effects of embedding the cluster in the two continua associated with the solid electrodes is made manifest.

To construct the desired model, we begin by imagining that the cluster calculations of the electronic structures of the tip and sample are carried out with boundary conditions that reproduce exactly the effective potential of the solid. Formally, such a potential can be constructed using standard projection operator techniques; in practice, there has been a great deal of effort invested in developing approximate embedding methods of varying rigor and quality. We will proceed with an analysis assuming that an exact embedding calculation has been performed, and then evaluate how closely our actual procedure conforms to what would be obtained in the ideal case. The comparison of our results with the ideal case is accomplished by systematically increasing the size of the model system and observing the effects on the computed coupling matrix elements. While rigorous convergence is difficult to demonstrate (particularly for the platinum tip, where the geometry is not known with accuracy), examining the behavior of the relevant computed quantities as a function of cluster size provides a heuristic estimation of the uncertainty inherent in our protocol. As illustrated in Tables 4 and 5, our results exhibit a significant degree of convergence for the tip sizes used.

Consider first the electronic structure of the tip. The first step is to compute the orbitals of the tip cluster with the exact embedding potential. This yields a set of one particle states, $\{\Psi_n^t\}$, which are filled up to the Fermi level of the cluster. Because the cluster is of finite size, its electronic structure does not form a continuum of states and there is a nontrivial spacing between the occupied orbitals of the cluster. For the purposes of our argument, what is specifically required is that there is a sufficiently large spacing between the highest occupied orbital with nonnegligible overlap with the sample orbitals and the next lowest orbital that has such a nonnegligible overlap. Orbitals that have effectively zero overlap with the sample are not relevant to the calculation of the tunneling matrix element. If there are two or more orbitals of the tip that overlap with the orbitals of the sample, are high enough in energy, and have an energy splitting that is small (compared to kT), each orbital's coupling with those of the sample must be explicitly calculated. The calculation then becomes rather complex. For the moment we shall assume that only one orbital lies high enough in energy and overlaps with the orbitals of the sample. Later on, we will argue that unless the close lying orbitals have a different orientation with regard to the sample orbitals, one can still use excitation out of a single orbital to determine the relative tunneling current. While the aforementioned complications can be avoided in most cases, it is important in establishing the validity of the cluster approach that it behave reasonably in the limit of a very large cluster where such complications would most likely occur.

We now construct approximate eigenstates of the full tip system as follows. First, we construct one particle orbitals for the solid electrode with the cluster removed, again replacing the tip cluster with an exact embedding potential. This leads to a set of states $\{\Psi_m^t\}$. The one particle orbitals of the entire system can then be written as a linear combination of the orbitals from the two fragments, subject to renormalization. If one views

the eigenstates of the solid electrode with the cluster removed and the tip cluster with the embedding boundary conditions as basis functions, then the eigenstates of the entire tip would most generally be represented by a linear combination of all of the functions from both regions. However, because the eigenstates of the tip cluster are assumed to be well separated in energy, and are also assumed to be nearly identical to the eigenstates of the tip calculated using the entire tip system (due to the use of an exact embedding potential) in that they do not strongly mix with other states in the solid electrode, we can, to a very good approximation, represent all of the eigenstates of the entire tip as linear combinations of a single eigenstate of the solid electrode and a single eigenstate of the tip cluster. Note that the least accurate aspect of this approximation, which is the use of a single eigenstate of the electrode (due to the fact that these eigenstates have smaller energy gaps), is irrelevant to the argument that follows; we can instead imagine producing a new set of electrode functions such that only one of them is required to build a specified eigenstate of the full system. Formally the full system eigenstates then have the form

$$\Phi^{t}_{k} = C^{n}_{k}\Psi^{t}_{n} + C^{m}_{k}\Psi^{t}_{m} \tag{3}$$

A similar construction can be performed for the sample. This leads to a set of single particle orbitals for the sample of the form

$$\Phi^{s}_{l} = C^{n}_{l}\Psi^{s}_{n} + C^{m}_{l}\Psi^{s}_{m} \tag{4}$$

We now evaluate eq 1 explicitly using the forms developed in equations 3 and 4. The resulting expression is

$$P_{t\rightarrow s} = \frac{2\pi}{\eta}\sum_{k}\sum_{k'}\int |\langle a_k\Phi^{t}_{k} + b_k\Phi^{s}_{k}|H|c_{k'}\Phi^{t}_{k'} + d_{k'}\Phi^{s}_{k'}\rangle|^2 f_{kk'}(E)\,dE \tag{5}$$

We now use the fact that we can neglect all orbitals of the tip that have zero overlap with the sample, and all orbitals of the sample that have zero overlap with the tip. The overlap between a tip and sample eigenfunction is then presumed to depend only upon the cluster part of the wave function. This is the central physical approximation, which presumably should become rigorous in the limit that the size of the clusters is increased. Factoring out the cluster matrix element yields the result

$$P_{t\rightarrow s} = \frac{2\pi}{\eta}|\langle\Psi^{t}_{n}|H|\Psi^{s}_{n}\rangle|^2\sum_{k}\sum_{k'}\int |C^{t}_{k}C^{s}_{k'}|^2 f_{kk'}(E)\,dE \tag{6}$$

In this expression, the dependence of the rate upon the position of the tip relative to the sample has been reduced to precisely the value of the cluster diabatic matrix element (in a noninteracting single particle model) between charge localized states on the tip and sample. The remaining multiplicative term, which certainly influences the absolute value of the current, is invariant with respect to the tip position. Thus, if the approximations used to arrive at eq 6 are valid, we can use ab initio quantum chemical cluster calculations to model the contrast in STM images.

We now proceed to a more general argument in which the assumption of a single cluster orbital that has a large tip−sample overlap and is well separated in energy from other such orbitals is relaxed. Consider first the tip. As the size of the cluster of metal atoms in the tip is increased, the single highest energy state in the small cluster dominating the tip−sample overlap will be broadened into a manifold of levels. Each state in the manifold will contain a (smaller) component of the overlap, and all states in the manifold will have slightly different energies. At first glance, it would seem that one would have to perform cluster calculations of the diabatic matrix element for each state in this manifold, removing an electron from each in turn. However, as long as each orbital in the manifold interacts in the same way with the sample (and this will be the case if the dominant contribution to the overlap still arises from the localized orbitals on the atoms of the tip closest to the sample), the relative value of the total matrix element will be properly estimated from a single cluster calculation. That is, each orbital in the manifold will be shifted in exactly the same way for any movement of the tip. Thus, the relative change in the matrix element for any given orbital in the manifold will be identical with the relative change in the value of the total matrix element. Formally we can then rewrite eq 5, where $f_{kk'}(E)$ now includes all additional contributions from the remaining states of the tip manifold, and where we have made explicit the assumption that that the dominant contribution in the manifold arises from a single localized wave function. Again factoring out the overlap of this localized wave function with the sample, we obtain a modified form of eq 6. Similar arguments can be made for the sample, although here such arguments may not even be necessary if the orbitals of the adsorbed molecule are well separated from those of the graphite electrode.

B. Computation of the Tunneling Matrix Elements. Given the approximations outlined in the preceding section, the tunneling current is directly related to the degree of electronic coupling between cluster representations of the tip and the sample. In an electron-transfer framework, this current is proportional to the square of the tunneling matrix element,[9] which represents the coupling between the two distinct quantum states, one with the electron localized on the tip and the other with the electron localized on the adsorbate−surface complex. The calculation of the tunneling matrix element is divided into two parts. In the first part, initial and final wave functions are generated. The initial wave function is composed of the wave function of the neutral adsorbate−surface complex combined with the wave function of the tip with an extra electron. The final wave function is composed of the wave function of the adsorbate−surface complex with an extra electron combined with the wave function of the neutral tip. The wave functions are generated by performing four SCF calculations in the absence of any external field. Calculations that included the external field did not alter the relative contrast of the STM images in the test cases studied. Two calculations are performed for the tip, one for its neutral state and one for the state of the tip with the extra electron, and two calculations are performed for the adsorbate−surface complex, one in its neutral state and one for the state of the complex with an extra electron.

The second part of the computation involves the calculation of the tunneling matrix element. The details of this calculation have been described elsewhere and will only be summarized here.[10] The difference between the calculations used here and standard electron-transfer calculations is the introduction of an external voltage into the Hamiltonian, as explained below.

The tunneling matrix element is given by

$$T_{if} = \frac{H_{fi} - S_{if}H_{ii}}{1 - S^2_{if}} \tag{7}$$

where

$$H_{fi} = \langle Y_f|H|\Psi_i\rangle \tag{8}$$

$$H_{ii} = \langle Y_i|H|\Psi_i\rangle \quad (9)$$

$$S_{if} = \langle Y_i|\Psi_f\rangle \quad (10)$$

and

$$H = h + \sum_b J_b - \sum_b K_b - \sum_i \mathbf{E}\cdot\mathbf{r}_i \quad (11)$$

where h is the one electron Hamiltonian, J is the Coulomb operator and K is the exchange operator. The first part of the Hamiltonian is composed of the Fock operator, which accounts for the electron−electron repulsion and the electron−nuclear attraction. The final term accounts for the interaction of the electrons with the external field, where **E** is the external electric field and $\mathbf{r}_i$ is the position of the electrons in the field. The external field is assumed to be constant and homogeneous with the field lines oriented perpendicular to the surface. The voltage applied across the tip−sample gap is 1−2 V, typical voltages in STM experiments in which adsorbate layers are studied and consistent with the experimental values to which the results are compared. The calculations were performed for a positive sample bias, corresponding to the electron tunneling from the tip to the adsorbate−surface complex.

Basis Set Dependence. Computational constraints required the use of the LAV3P basis set[11,12] for the Pt atoms, which uses an effective core potential to construct the basis functions of inner shell electrons for the Pt atoms. The basis set dependence of the tunneling matrix element was then evaluated by testing the 6-31G, 6-31G*, cc-pVDZ(-d), and cc-pVTZ(-f) basis sets for the remaining atoms. The matrix elements were obtained by positioning a four-atom Pt tip above the Cl atom in a chlorinated alkane, which lies above a single layer of graphite. (The choice of tip structure, surface structure, and tip−adsorbate spacing is discussed below.) The matrix element values, given in Table 1, indicate that including polarization functions on the non-hydrogen atoms has a negligible effect on the computed matrix element. Using the double-ζ and triple-ζ basis sets, however, results in a significant change in the calculated values of the transfer matrix element. To ensure that the basis set is adequately converged it is therefore necessary to use the cc-pVTZ(-f) basis set. The use of larger basis sets is not computationally feasible at the present time.

To reduce the necessary computational effort, the use of mixed basis sets was then investigated. The effects of using a smaller basis set for the underlying graphite surface and for the carbons and hydrogens of the adsorbate are illustrated in Table 2. The results show that the use of the cc-pVTZ(-f) basis set for the adsorbate alone accurately reproduces the values obtained when the cc-pVTZ(-f) basis set is used for all the atoms. Hence, all subsequent calculations utilize the cc-pVTZ(-f) basis for the adsorbate and the 6-31G basis set for all other atoms. As the cc-pVTZ(-f) basis set has not yet been incorporated in our program for bromine and iodine atoms, brominated and iodinated alkanes used the LAV3P basis set for the bromine/iodine atoms while all other atoms were modeled using the 6-31G basis set.

The computations employed the JAGUAR suite of electronic structure programs.[13] The diabatic localized wave functions of the two diabatic states are evaluated directly, and the off-diagonal transfer matrix element of the Hamiltonian between these wave functions is then calculated. The latter task is recast in the form of a Fock matrix assembly and a pseudodensity matrix is then constructed. Utilizing a pseudospectral formulation of Hartree−Fock theory,[14−17] JAGUAR is able to significantly reduce the time required for the calculation of the coupling matrix elements. Typical CPU times for SCF and matrix element calculations are presented in Table 3. The required computational effort is estimated to be 1−2 orders of magnitude less than what would be required using conventional ab initio programs and methods for a system of this size.

TABLE 1: Basis Set Dependence of Calculated Matrix Elements at 1 V Bias Voltage for $CH_3CH_2CH_2CH_2Cl$ Adsorbed on Graphite

basis set	6-31G	6-31G*	cc-pVDZ(-d)	cc-pVTZ(-f)
# basis functions	600	845	965	1563
matrix element (cm^{-1})	3.49	4.17	9.21	16.61

TABLE 2: Dependence of Matrix Elements on the Size of the Basis Set

basis set (all other atoms use 6-31G basis.)	cc-pVTZ(-f) Cl only	cc-pVTZ(-f) adsorbate only	cc-pVTZ(-f) all atoms
# basis functions	625	877	1563
matrix element (cm^{-1})	9.08	16.35	16.61

TABLE 3: Typical CPU Times

type of calc.	# basis functions	CPU time
SCF	801	9.96 h.
matrix element	877	4.15 h.

Presentation of the Data. In presenting contrast images, the variation of the square of the tunneling matrix element as the tip is translated over the atoms in the adsorbate is presented in the plots that follow. The square of the matrix element is taken to be a measure of the tunneling current. For convenience, the squared matrix elements are scaled by the largest value occurring for each type of molecule. However, this scaling is unique to each terminal functional group. Thus, a valid comparison can be made between the plots of the different conformations of molecules with the same terminal functional group only. In making any other comparison, one must realize that the scaling changes from one terminal functional group to the next. The plots are meant only to illustrate the contrast variation that is apparent within an individual molecule and how the variation changes in different conformations. The range of values for the matrix elements is inset in the upper right corner of each plot in order to facilitate any qualitative comparisons between different molecules. All plots are calculated at a bias voltage of 1.5 V unless otherwise indicated. The calculations of the matrix elements in this study were performed at constant height. The correlation between constant-height and constant-current images will be discussed in section V.

III. Physical Model of the STM Interface

For the purposes of evaluating the feasibility of the current theoretical approach, it is considered sufficient if the calculated points accurately reproduce the most outstanding features of the experimental images. Thus, the calculated plots should reproduce the bright and dark extremes of the experimental images but need not reproduce the more subtle features. In particular, no differentiation between the carbons and hydrogens is noticeable in the calculated plots.

Tip Structure. The effect of the tip structure on the transfer matrix element was examined by calculating the matrix elements for an eight-carbon long thiol ($C_8H_{17}SH$) for various tip structures. Sautet et al.[18] previously studied the effects of varying the tip structure on the STM image of sulfur on Re, but they did not reach any definitive conclusion as to the optimal tip structure appropriate for the general case. In the current study,

TABLE 4: Average Matrix Elements (cm^{-1}) for the Molecule $CH_3(CH_2)_7SH$ at a Tip Height of 7.4 Å above the Surface

functional group	1-atom tip	3-atom tip	4-atom tip	5-atom tip
SH	430.80	6.38	249.41	123.49
CH_2	339.70	12.67	139.71	67.97
CH_2	142.57	13.23	12.98	13.14
CH_2	122.69	6.56	167.21	111.72
CH_2	155.87	4.03	133.81	114.52
CH_2	111.93	6.47	31.72	12.95
CH_2	188.78	11.22	59.26	27.58
CH_2	120.85	11.74	221.73	118.60
CH_3	150.66	6.33	213.07	143.85

TABLE 5: Average Matrix Elements (cm^{-1}) for the Molecule $CH_3(CH_2)_7SH$ at a Tip Height of 10.4 Å above the Surface

functional group	1-atom tip	3-atom tip	4-atom tip	5-atom tip
SH	53.17	0.35	33.23	19.92
CH_2	40.31	0.69	32.84	20.27
CH_2	13.04	0.59	13.25	8.10
CH_2	15.45	0.42	15.53	11.25
CH_2	9.38	0.27	5.81	6.07
CH_2	13.82	0.05	8.16	5.62
CH_2	19.86	0.48	11.82	7.13
CH_2	10.31	0.51	15.89	10.52
CH_3	31.40	0.19	7.30	5.78

the tip is assumed to be composed of a cluster of Pt atoms. The cluster sizes examined range from one Pt atom to five Pt atoms. The three-atom tip geometry is an isosceles triangle oriented parallel to the surface, and the four-atom tip is a tetrahedron with the apex pointed toward the surface. The five-atom tip has a trigonal bipyramidal structure. The calculations of the matrix elements were performed for two different tip heights in order to determine if the Pt atoms above the first layer of the cluster were interacting with the surface. The lower tip height of 7.4 Å corresponds to a Pt−S distance approximately equal to the sum of their respective covalent radii.

The matrix elements are presented in Tables 4 and 5. A comparison of the matrix elements above the terminal CH_2SH with the matrix elements above the rest of the chain is used in determining the relative contrast of the sulfur end of the molecule and the remainder of the carbon chain. At a tip height of 7.4 Å, the one-atom, four-atom, and five-atom tip values indicate that the thiol end of the molecule has a higher average matrix element than the rest of the chain. However, the ratio of the sulfur end of the molecule to the rest of the chain differs significantly between the one and four-atom tips. The four- and five-atom tips, however, yield similar values for the ratio of the sulfur end of the molecules to the rest of the chain. Similarly, the four- and five-atom tips show the same qualitative variation in the value of the matrix element along the carbon chain. The one-atom tip does not show any such variation. The three-atom tip shows no significant difference between the two sides of the molecule. The discrepancy between the one-atom tip values on one hand and the four and five-atom tip values on the other hand indicates that the second layer of Pt atoms is interacting with the molecule. A cursory glance at Table 5 indicates that when the tip is retracted to a distance of 10.4 Å above the surface, the qualitative discrepancy between the one-atom and the four- and five-atom tip structures vanishes. At the higher tip distance, the second layer of Pt atoms plays a far less significant role in the calculation of the matrix elements.

TABLE 6: Energies of Interaction as a Function of Tip-adsorbate Distance and Tip Structure

atom−tip distance (Å)	1-atom tip (eV)	4-atom tip (eV)
14.4	−0.002	−0.05
13.4	−0.002	−0.05
12.4	−0.004	−0.05
11.4	−0.007	−0.06
10.4	−0.02	−0.07
9.4	−0.05	−0.11
8.4	−0.18	−0.28
7.4	−0.41	+0.07

TABLE 7: Average Matrix Elements (cm^{-1}) for the Molecule $CH_3CH_2CH_2CH_2SH$ as a Function of the Number of Surface Layers

functional group	no graphite	1 layer	2 layers
SH	313.69	1.68	6.88
CH_2	1943.35	3.90	9.54
CH_2	2771.23	2.51	4.13
CH_2	961.90	1.55	3.53
CH_3	755.47	6.44	2.23

To verify that the second layer of Pt atoms interacts with the molecule, the energy of interaction between the tip and the adsorbate is presented in Table 6 for various heights of the tip above the sulfur atom. The results indicate that at a tip height of 7.4 Å the one-atom tip is still in an attractive regime while the four-atom tip has already entered a repulsive regime. This repulsive interaction is most likely responsible for reducing the value of the matrix elements when the four-atom tip is in the vicinity of the sulfur atom. Thus, the second layer of Pt atoms plays a significant role in determining the value of the matrix element. Although the third layer of Pt atoms does influence the values of the matrix elements, the ratio of the matrix elements above the functional group to those over the bulk of the chain does not vary significantly. Hence, a four-atom tip was used in all subsequent calculations.

Surface Structure. The effect of the surface structure on the transfer matrix elements was investigated by calculating the transfer matrix elements for a four-atom Pt tip above a four-carbon long thiol with no surface, with a single layer of graphite and with two layers of graphite. The results are presented in Table 7. The calculated values show a significant change in the value of the matrix elements when the first layer of graphite is introduced. When a second layer of graphite is introduced the matrix elements obtained are of the same order of magnitude as the one-layer results. However, the amplitudes of the matrix elements are modified; in particular, the one-layer calculation has a larger amplitude on the terminal carbon atom and a smaller amplitude on the sulfur, than is obtained for the two layer calculation.

We interpret the larger amplitude on the terminal carbon atom as an artifact that is due to insufficient delocalization of charge in a one-layer model with a short carbon chain. This artifact is also removed by employing a longer chain length, as is discussed in the subsection below. Because this problem disappears when a longer carbon chain is used, even in a single layer calculation, inclusion of a second layer to address this problem is not necessary. The diminishment of the amplitude of the matrix element when the tip is above the sulfur atom (although not for the carbon adjacent to it) is more difficult to understand quantitatively. A possible explanation is that the terminal carbon atom on the short chain is drawing off charge from this atom as well. Again, it is shown below that this problem is less prominent when a longer chain length is used.

Ideally, we would utilize both a second layer of graphite and a longer chain length in our calculations. However, this model is expensive computationally and also exhibited some convergence problems. In view of the fact that the single layer model exhibited qualitatively correct results (as compared to experiment, and also in accordance with the two layer calculations), we choose in this paper to report single layer calculations only. In future work, we intend to address the convergence problems and carry out quantitative benchmark computations with two layers and a long carbon chain. We believe, however, that the current results provide qualitatively reasonable estimations of the intensity ratios that can be profitably compared with the experimental data.

Chain Length. A comparison of the matrix elements for the short chain thiol with one layer of graphite, given in Table 7, with the matrix elements for the long chain thiol in Table 5 (4-atom tip) indicates that the additional atoms change the relative contrast of the atoms in the molecule. The long chain thiol shows a pronounced peak in the vicinity of the terminal thiol group while the short chain thiol shows a substantially less pronounced peak. The relative contrast of the long chain thiol is similar to the contrast shown by the two layer short chain thiol results presented in Table 7. However, the long chain thiol results show a more pronounced peak in the vicinity of the functional group. The use of a larger chain, and subsequently a larger graphite layer, thereby produces an effect similar to the use of a second layer of graphite with a short carbon chain. Hence, as was justified above, all subsequent calculations utilized a long chain molecule adsorbed on a single graphite layer.

Resolution. To determine the number of points required to reproduce the most prominent features of the experimental STM images, the following procedure was followed. A grid of points, with spacing of 0.2 Å between grid points, was used to generate the image (Figure 1a) of a short chain brominated alkane adsorbed on a single layer of graphite. The STM tip is composed of a tetrahedral cluster of Pt atoms and is at a bias voltage of 2 V relative to the surface. The results were then compared with the plot generated by sampling only points directly above atoms in the adsorbate (Figure 1b). Both figures show an increased brightness (increased tunneling probability) in the vicinity of the terminal CH_2Br group as the most prominent feature of the image. The comparison shows that sampling above atoms in the adsorbate adequately accounts for the most prominent features of the image. Therefore, the matrix elements for all subsequent molecules were only calculated with the tip directly over the atoms of the adsorbate.

Summary of Convergence Studies of the Physical Model and Connection with Embedding Analysis. In section II(A), our analysis assumed that we were calculating eigenstates of the tip and sample using embedding boundary conditions. In actual fact, we have instead used finite clusters either capped by hydrogens (sample) or simply terminated at a finite number of atoms (tip). However, in section II(A), we argued that if the quantity of interest (the diabatic tunneling matrix element) could be shown to be more or less converged with respect to increases in the size of the model, then the model was a satisfactory replacement for the use of embedding boundary conditions. Specifically, what such convergence demonstrates is precisely what was assumed in asserting the validity of eqs 3 and 4. Namely, as the cluster is increasingly coupled to the remainder of the system, the relevant frontier orbitals are not strongly mixed with other states of the tip and hence they do not qualitatively change the matrix element from what is being

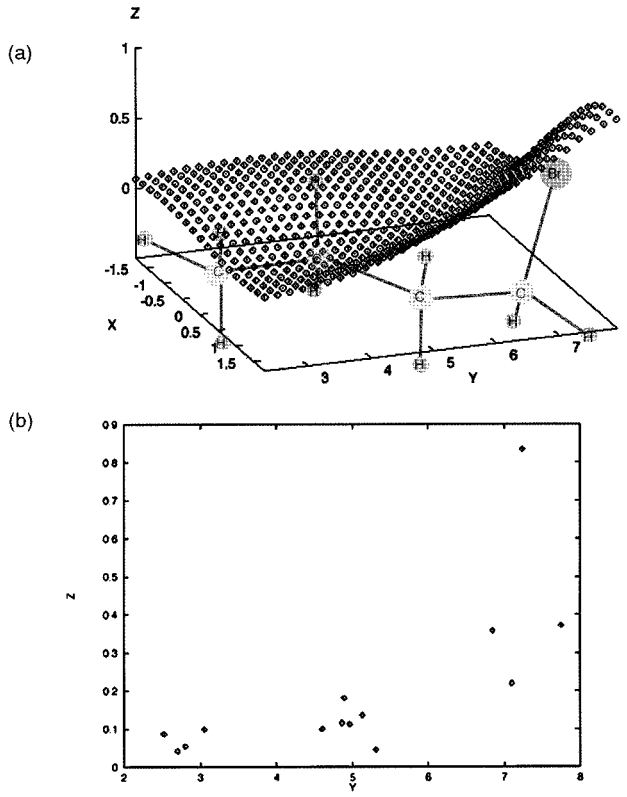

Figure 1. (a) Surface plot of squared matrix elements above C_4H_9Br. The *x, y* axes are length scales given in angstroms; *z* axis gives the scaled values of the squared matrix elements. (b) Projection of squared matrix element values directly above atoms in the adsorbate on the $y-z$ plane.

estimated in the cluster calculation. For the tip, the close agreement of the four- and five-atom tips provides evidence along these lines. Note the inadequacy of the single-atom tip, which clearly does not represent a good approximation to embedding boundary conditions. Similarly, note that for the sample the isolated molecule is also a qualitatively inadequate model, while the use of a single graphite layer, although not fully converged, is judged to be adequate for our purposes in this paper. Of course, these conclusions might be modified by more careful studies of larger and more realistic representations of either the tip or sample. On the other hand, the models we are using here are rather large when compared with other ab initio computations along these lines reported in the literature, and therefore constitute a reasonable starting point for a semiquantitative analysis, which is our goal in the present paper.

IV. Results

The starting geometries of the molecules adsorbed on graphite to be discussed have been obtained courtesy of William Goddard III. The geometry is first optimized for a single molecule on the graphite sheet. Two additional molecules are then added to simulate the packing arrangement of molecules on the surface and the geometry is reoptimized. This process is repeated for various chemical species.[7] The resulting optimized structures are used in all of the present calculations. The molecules are truncated at the desired chain length, and the dangling bonds are capped with hydrogen atoms. The surface is modeled using a truncated, single-layer graphite surface, with all dangling bonds capped with hydrogens. A typical adsorbate−surface complex is presented in Figure 2.

Alkanes. A single alkane molecule is imaged with its backbone parallel to the graphite surface. The plot is presented

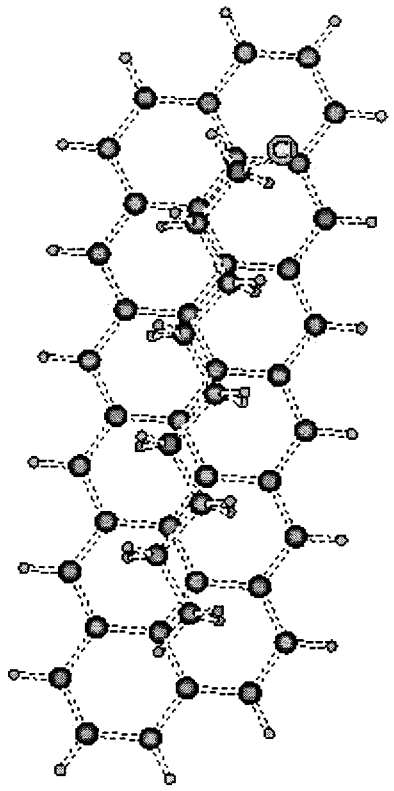

Figure 2. Schematic view (from above) of a halogenated alkane adsorbed on a graphite surface whose dangling bonds have been capped by H atoms.

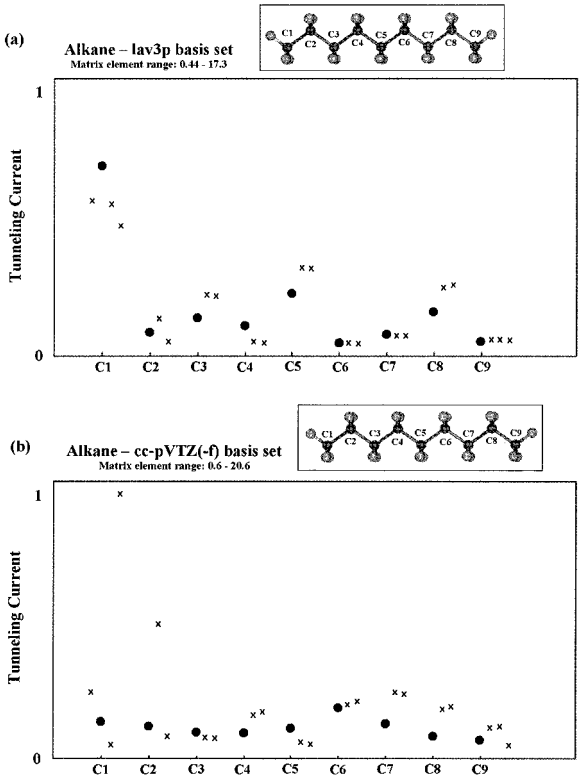

Figure 3. Plot of C_9H_{20} using (a) the LAV3P basis set and (b) the cc-pVTZ(-f) basis set. The *y*-axis gives the squared matrix element scaled by the largest value for the adsorbate. The *x*-axis indicates the atom over which the tip is situated.

in Figure 3. Figure 3a uses the 6-31G basis set while Figure 3b uses the cc-pVTZ(-f) basis set for the adsorbate. Figure 3a is considerably noisier than Figure 3b. Thus, the use of the larger basis set smoothes out the noise in the plot. With the exception of two or three data points, Figure 3b shows that the tunneling current is relatively uniform throughout the carbon chain. Additionally, the tunneling current follows a sinusoidal pattern as the tip scans across the chain. This pattern is consistent with experimental images that show slight variations in the magnitude of the tunneling current along the carbon chain due to the mismatch between the adsorbate and the underlying surface.

Halogenated Alkanes. Plots of halogenated alkanes adsorbed with their carbon backbone parallel to the graphite surface have been calculated at a tip height of 10.4 Å above the graphite surface. The results are presented in Figure 4a−f. The plots illustrate a clear distinction between the different conformations of the adsorbate. When the halogen atom points out of the plane of the carbon chain, the tunneling current is significantly enhanced in the vicinity of the functional group. The remainder of the chain is generally dark relative to the functional group. When the functional group lies in the plane of the carbon chain, the entire molecule appears to have a relatively constant matrix element value and the functional group does not generally exhibit any enhanced tunneling current.

Experimental STM images have shown that brominated and iodinated alkanes are "bright" in the vicinity of their functional group, signifying an increase in the tunneling current in this region of the molecule.[19] The calculated plots discussed above suggest that the experimental images correspond to molecular geometries in which the functional group points out of the plane of the carbon backbone toward the tip. The calculated results for the brominated alkanes agree with the recent work of Claypool et al.[20] The experimental images of the chlorinated alkanes do not show clear distinguishing features in the vicinity of the functional group. Similarly, the calculated plots of the chlorinated alkanes do not provide a clear qualitative distinction between the two conformations for this molecule. Further analysis is required in order to determine which of the two conformations is experimentally imaged. The issue of determining which of the different conformations appears in the experimental images will be further developed in section V.

Alcohols and Thiols. Thiols are imaged in two conformations: with the functional group in the plane of the carbon backbone and with the functional group pointing toward the tip. Only the conformation with the functional group pointed out of the plane shows some enhanced tunneling in the region of the sulfur atom, as shown in Figure 5a,b. This result is at odds with the findings of Faglioni et al.[7] who found that the sulfur appears bright in the flat conformation as well. However, the range of matrix elements in both the up and flat conformations is quite similar. In section V the difference between the two thiol conformations will be addressed in greater detail.

The squared matrix elements of an adsorbed alcohol molecule are plotted in Figure 6. The OH functional group, lying in the plane of the carbon backbone, is slightly darker than the rest of the chain, as in the experimental images.[21] Although there is a great deal of noise in the plot, the range of matrix element values is extremely small.

Amines. Amines are imaged in three conformations. Of the three conformations shown in Figure 7a−c, the structure with one of the hydrogens of the NH_2 group pointed toward the tip and one in the plane of the carbon chain (amine up) is most consistent with the experimental results, with very small variations in matrix element values along the length of the

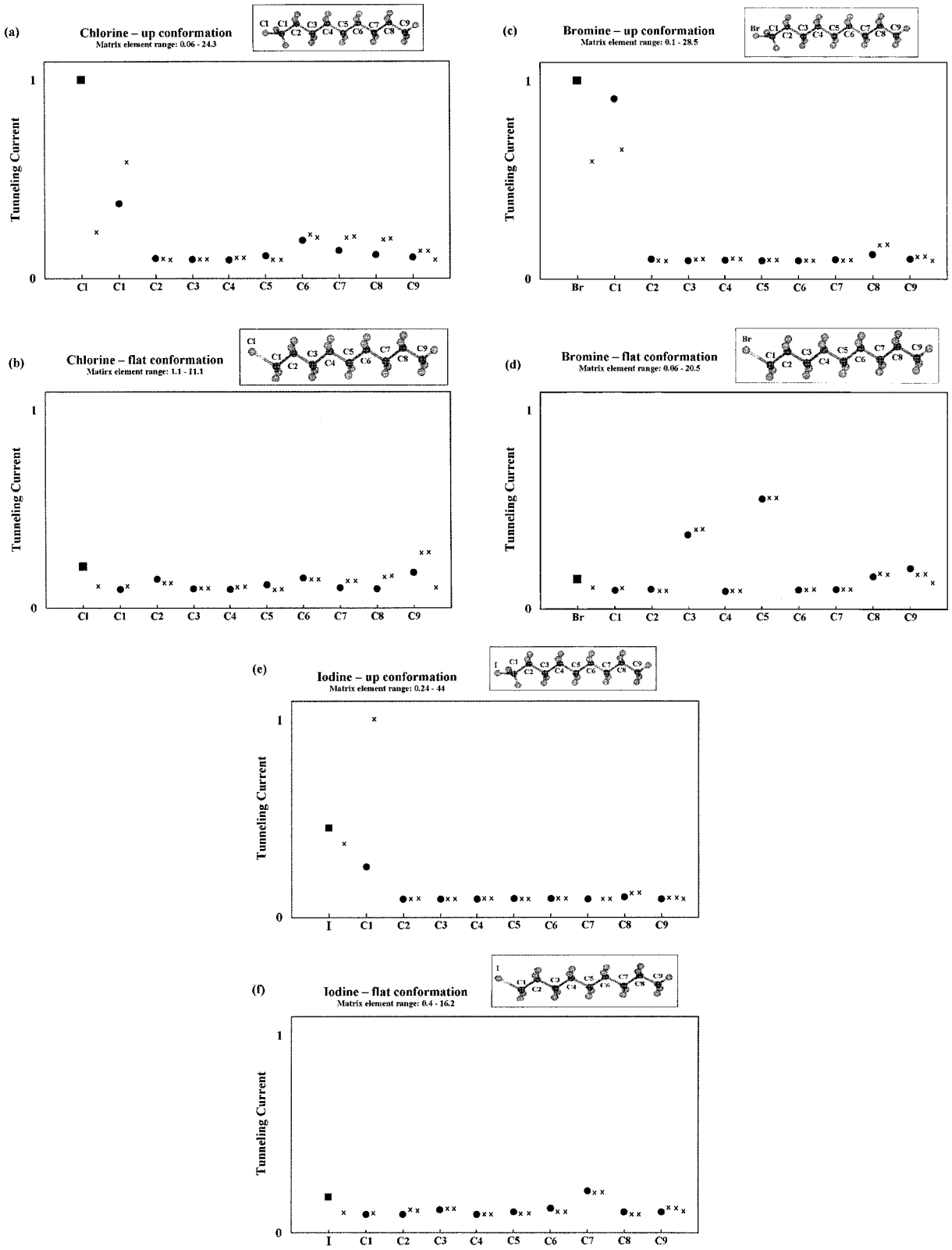

Figure 4. Plots of C9H19R (R = Cl, Br, I). The *y*-axis gives the squared matrix element scaled by the largest value for the adsorbate. The *x*-axis indicates the atom over which the tip is situated. (a) R = Cl in the up conformation; (b) R = Cl in the flat conformation. (c) R = Br in the up conformation; (d) R = Br in the flat conformation. (e) R = I in the up conformation; (f) R = I in the flat conformation.

molecule. The amine down and amine flat plots show some additional variation along the length of the chain. However, the comparison of theory with experiment is particularly difficult in the case of the amines due to the variation in intensity of different parts of the molecule in different areas of the experimental images (Moire pattern).[19] This variation is an interference pattern arising from the mismatch of the molecule with the underlying graphite substrate. Hydrogen bonding within the monolayer of amines may also alter the geometries and the expected STM image. A more accurate determination of their structure may require that these additional effects be taken into account in the computations, which are currently limited to a

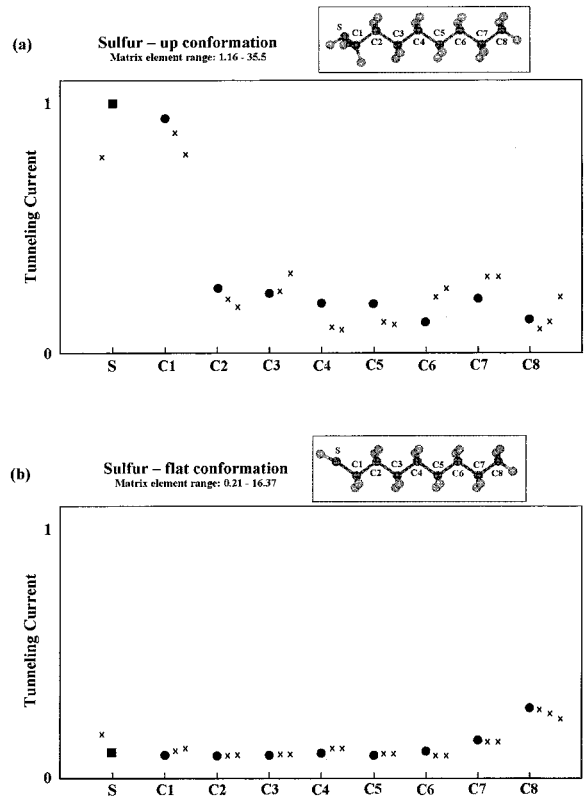

Figure 5. Plots of $C_8H_{17}SH$. The *y*-axis gives the squared matrix element scaled by the largest value for the adsorbate. The *x*-axis indicates the atom over which the tip is situated. (a) SH in the up conformation; (b) SH in the flat conformation.

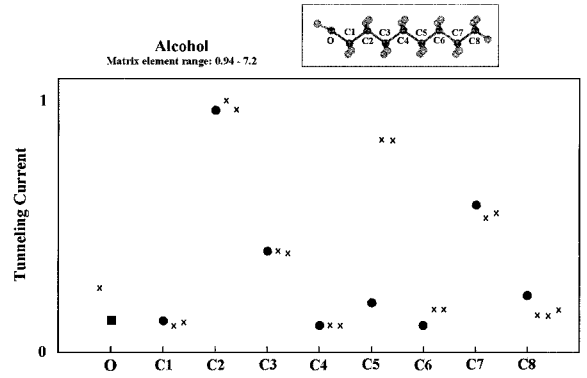

Figure 6. Plot of $C_8H_{17}OH$ in a flat orientation. The *y*-axis gives the squared matrix element scaled by the largest value for the adsorbate. The *x*-axis indicates the atom over which the tip is situated.

single adsorbate molecule. Nevertheless, a more quantitative analysis can more accurately determine the conformation that appears in the STM images.

V. Quantitative Comparison with Experiment

To determine the molecular conformations appearing in experimental images more conclusively, a more quantitative comparison with experiment is called for. However, a quantitative comparison with experimental results is complicated by the fact that the experimental images are observed in the constant current mode of the STM, while the preceding calculations are performed at constant height. When obtained at constant height, the image is a map of changes in the tunneling current; at constant current, the images are a map of the changes in the tip height. One can assume that the tunneling current decays exponentially as the tip is moved away from the surface. This

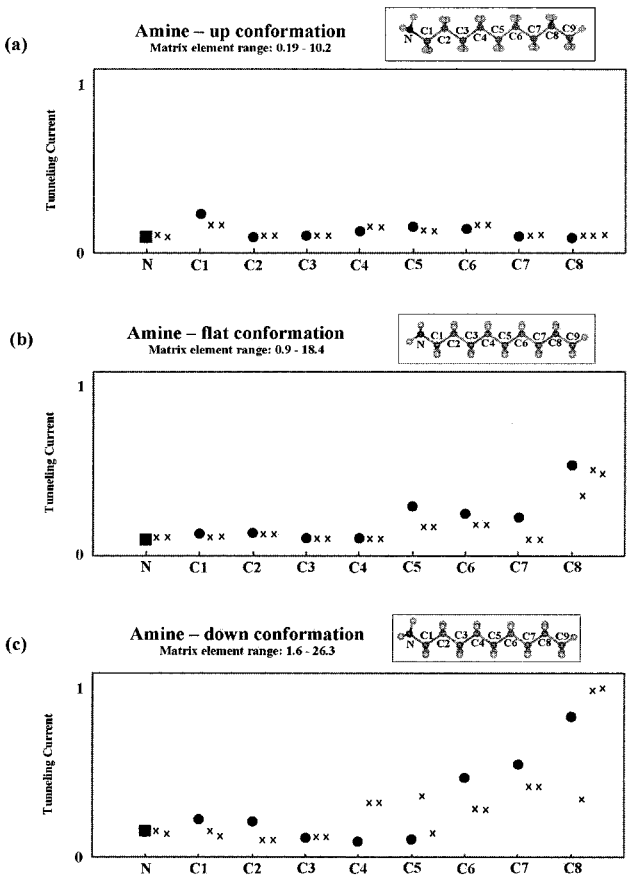

Figure 7. Plots of $C_8H_{17}NH_2$. The *y*-axis gives the squared matrix element scaled by the largest value for the adsorbate. The *x*-axis indicates the atom over which the tip is situated. (a) Amine in the up orientation = one H atom pointed toward the tip and one H atom in the plane of the carbon backbone. (b) Amine in the flat orientation = one H atom pointed toward the tip and one H atom pointed toward the surface. (c) Amine in the down orientation = one H in the plane of the carbon backbone and one H atom pointed toward the surface.

assumption is valid only for the modeling of nonresonant tunneling.[22] However, as Figure 8a−f illustrates, an exponential decay is indeed observed as the tip is retracted from the surface. Thus, one can assume that the current simulations are performed in the nonresonant tunneling regime. Utilizing this fact, a method to more quantitatively relate the calculated plots of squared matrix elements to the experimentally obtained constant current images of the STM can be devised.

To make a quantitative comparison with experiment, two regions on each molecule are chosen as representative of the functional group and the bulk of the chain, respectively. The tunneling matrix element is then calculated at various tip heights over these two regions. These points are now fit to an exponential functional form in order to enable one to translate a constant height image into a constant current image. The exponential function is generated by performing a two parameter fit to a logarithmic function (i.e., tip height = f(matrix element) = ln(matrix element) + C). The fitting is performed twice, once for each region of the molecule. Some typical examples of the fitting are shown in Figure 8. While some plots exhibit more variance than others from an exponential functional form, the overall quality of the fits is quite reasonable and adequate for the purposes of the present paper, which is a semiquantitative comparison of theory and experiment. Using the generated functions, the variation in the matrix elements can be transformed into the variation of the tip height above the surface.

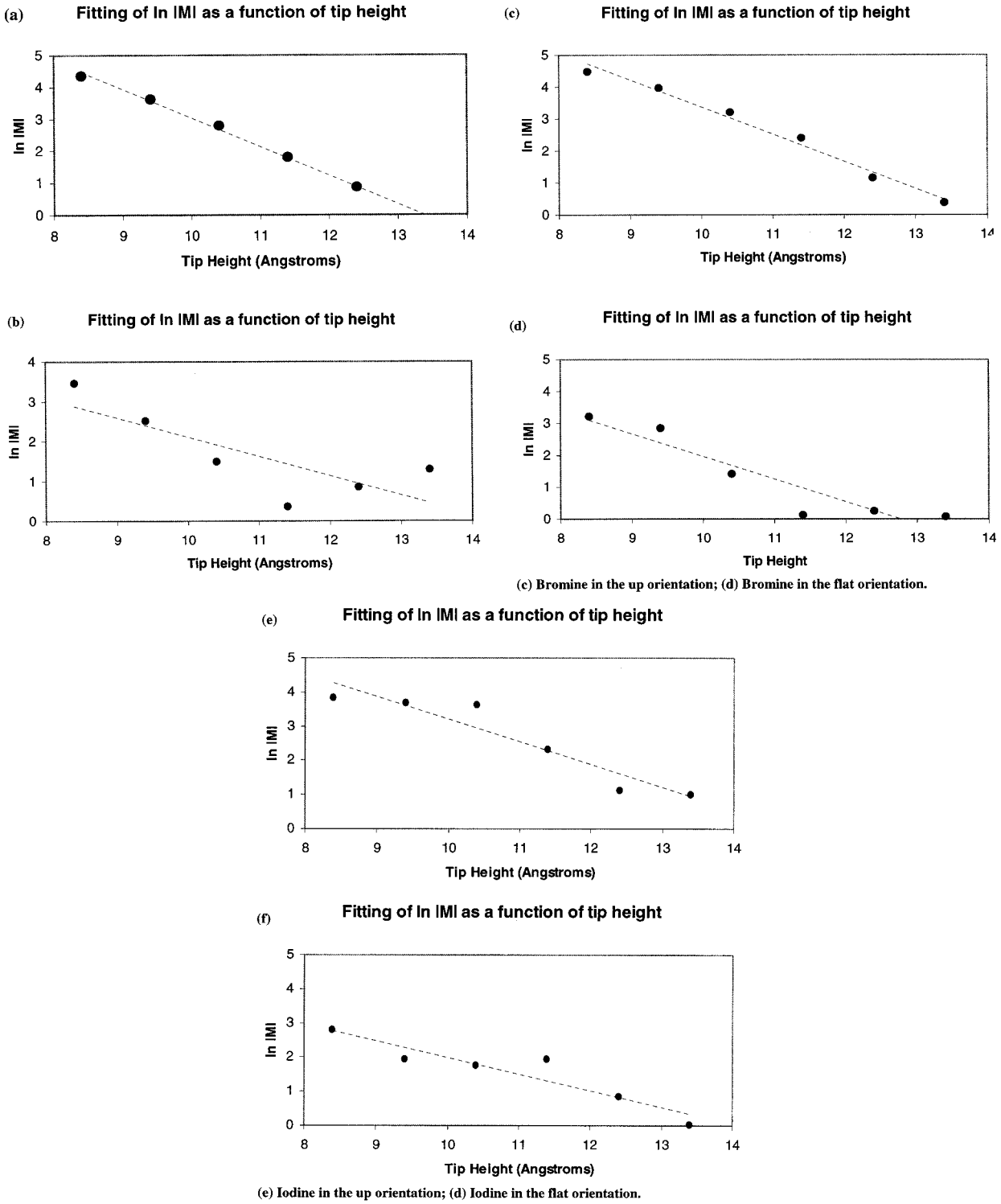

Figure 8. Examples illustrating the exponential decay of tunneling current as a function of tip height for: (a) chlorine in the up orientation; (b) chlorine in the flat orientation; (c) bromine in the up orientation; (d) bromine in the flat orientation; (e) iodine in the up orientation; (d) iodine in the flat orientation.

The quantitative measure used for the STM images is a ratio of the "brightness" of the functional group region to the rest of the chain.[19] However, to make a valid comparison with the experimental images, a more accurate understanding of the mechanism used by the STM to generate constant current images is necessary.

In generating constant current images, the bias voltage and set-point current are determined by manual input. The STM first moves the tip to an initial position above the sample that matches the input parameters. It is important to emphasize that the absolute height of the tip above the sample is unknown and is not determined experimentally. Rather, the STM translates the tip across the sample, allowing the piezo element to move the tip closer to or farther from the sample at each point in the sweep in order to maintain a constant current (Figure 9a). The data recorded by the STM is the displacement of the tip from its initial position. The STM image thus maps the change in the tip height relative to its initial position. Images appear bright or dark relative to this initial position (Figure 9b).

In performing theoretical calculations, the tip height is clearly

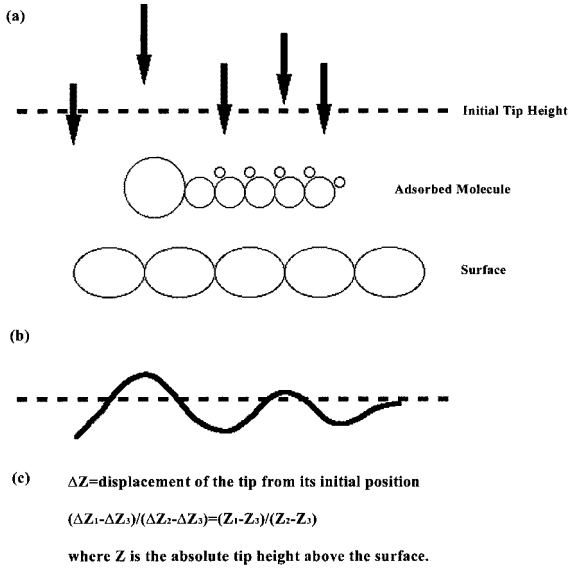

Figure 9. (a) Schematic of the operation of the STM in constant current mode. (b) Topographic image generated by movement of the tip in (a) displayed relative to the initial tip position. (c) Equivalence of the ratio of relative tip displacement with the ratio of absolute tip heights used in the calculation.

TABLE 8: Parameters Used in the Calculation

functional group	exptl. ratio[19]	accepted ratio (calculation)
OH	1.0	$0.6 < OH < 1.05$
Cl	1.0	$0.7 < Cl < 1.05$
NH_2	1.3	$1.1 < NH_2 < 1.43$
Br	2.0	$1.8 < Br < 2.2$
I	3.0	$2.7 < I < 3.3$
SH	3.1	$2.7 < S < 3.4$

known. What is unknown is the absolute tip height that corresponds to the initial position used by the STM. In comparing the calculated values to the experimental images, it is the changes in tip height, ΔZ, relative to the initial tip height that need to be calculated. Additionally, in the work of Cyr et al.[19] the ratio of the functional group to the rest of the chain is determined by subtracting the displacement of the tip (relative to the initial tip height) over a trough region in the image from both the numerator and denominator of the desired ratio. The ratio now becomes the change in tip displacement between the functional group and the trough region, relative to the change in tip displacement between the bulk of the chain and the trough region. The change in the displacement of the tip, relative to the initial tip position, between two regions of the molecule is the same as the change in the absolute tip heights over the two given regions (see Figure 9c).

Thus, to make a valid comparison with the experimentally determined ratios, which are presented in Table 8, the tip height over the trough regions must be determined. However, this information is not readily available from the performed calculations, as the trough regions roughly correspond to the regions between adjacent molecules. Therefore, the tip height above the trough region, Z_3, is treated as an adjustable parameter. The ratio is then calculated by the following procedure. A value for the transfer matrix element is chosen between 5 and 200 wavenumbers. Utilizing the previously determined logarithmic functions for the tip height, the selected value of the transfer matrix element yields the tip heights at the functional group, Z_1, and over the bulk of the chain, Z_2. Z_3 is then allowed to vary. Because the experimentally used Z_3 lies over a dark region of the image, the tip must be closer to the surface than when it is over the bulk of the chain. The calculated values of the tip height over the bulk of the chain are all found to be greater than ~9 angstroms. In the calculations, Z_3 is therefore allowed to assume values between 6 and 9 angstroms, tip heights that would correspond to dark regions of the images sampled. For every value of Z_3, the ratio $R = (Z_1 - Z_3)/(Z_2 - Z_3)$ is then calculated. Each value of the transfer matrix element gives a range of values for R, corresponding to the different values of Z_3. The procedure is then repeated for a grid of values of the transfer matrix element between 5 and 200 wavenumbers. In determining acceptable agreement with experiment, we allow for errors in both the calculations and the measurements; our allowed range for the computed ratios for each functional group, which is estimated heuristically, is presented in Table 8.

Table 9 records the locus of values of Z_3 at each value of the transfer matrix element for which the calculated ratio falls within the accepted ranges given in Table 8. As Table 9 illustrates, most molecular conformations studied have a region of matrix elements and values of Z_3 that yield ratios consistent with the experimentally determined ratios. The chlorine in the up conformation does not have any values that yield the experimental ratios, indicating that this conformation is most likely not consistent with the experimental images or that intermolecular interactions within the imaged monolayers, which are not included in the calculation, may play a more prominent role in the generation of the STM images. Utilizing the data presented in Table 9 and the plots of the preceding section allows one to make more conclusive determinations regarding the molecular conformations present in the STM images.

A more complete comparison between the calculated values and the constant current images requires a more detailed understanding of the relationship between the transfer matrix element and the tunneling current. This study began with the ansatz that the tunneling current is directly proportional to the square of the tunneling matrix element. If the constant of proportionality is assumed not to vary from system to system, then for any observed tunneling current there exists only one value of the transfer matrix element, and this value is the same for all systems studied at the same tunneling current. Utilizing this assumption, the value of the transfer matrix element that corresponds to the experimentally observed images can be estimated. A cursory glance at Table 9 shows that there is only a small region of values of the transfer matrix element that yield ratios consistent with experimental results. In particular, only in the range 5 to 20 wavenumbers can suitable values of Z_3 be found for all the adsorbates discussed above. A value of between 6 and 8 angstroms for Z_3 then satisfies the acceptance criteria of most of the adsorbates studied for this region of matrix elements. Indeed, Z_3 is not expected to vary significantly from system to system because the trough regions, which correspond to the positions between terminal methyl groups of adjacent molecules in the STM images, lie far enough away from the bright or dark functional groups that their tunneling intensities are not expected to be altered when the functional group is changed.

The results presented in Table 9 indicate that the chlorine and thiol end groups lie in the plane of the carbon backbone while the bromine end group points toward the tip. This result for the thiol functionality is now consistent with the results of Faglioni et al.[7] Only the amine down conformation yields results consistent with the experimental images. The results for the iodinated alkanes are less conclusive. Both the up and flat conformations yield values that are consistent with the experimental images. However, the plots of the previous section tend

TABLE 9: Values of Z_3 (Å) that Are within the Parameter Limits for Wavenumbers Ranging from 5 to 200

M. E. range	5−20	21−35	36−50	51−65	66−80	81−95	96−110	111−125	126−140	141−155	156−170	171−185	186−200
Cl (u)													
Cl (f)	6−9												
Br (u)	6												
Br (f)													
I (u)	8.7−9	8.2−8.8	7.4−8.2	7.3−8.0	7.3−7.8	7.2−7.3	7.0−7.2	6.9−7.0	6.8	6.7	6.6	6.5	6.4
I (f)	7.3−9.0	6.4−7.2	6.0−6.4										
SH (u)		8.5−9	8−8.5	7.6−8	7.4−7.7	7.2−7.5	7−7.3	6.8−7.1	6.7−6.9	6.5−6.8	6.4−6.7	6.3−6.6	6.2−6.5
SH (f)	6.9−8.8	6.2−6.9	6.0−6.1										
OH	6−6.7												
NH_2 (u)	-												
NH_2 (d)	6−9												
NH_2 (f)													

to suggest that the iodine up conformation is the more probable conformation appearing in the experimental images.

The assumption that the constant of proportionality does not change from system to system is therefore crucial in making more complete comparisons. The validity of this assumption has yet to be investigated. Additionally, experimental factors, such as the use of different tips, may further complicate a more complete quantitative comparison. However, by combining the qualitative plots of the previous section with an analysis of the values of Z_3 consistent with the calculations, one can arrive at a more informed guess as to the absolute conformation of the molecule in question.

VI. Discussion

The results indicate that chlorine and thiol functionalities lie in the plane of the carbon backbone, while the bromine and iodine functionalities are pointed out of the plane of the backbone toward the tip. These findings suggest a correlation between the size of the terminal functional group and its position relative to the surface. The chlorine and sulfur groups are small enough to orient themselves in the plane of the carbon backbone near the surface, while the bromine and iodine groups are too large to lie close to the surface and therefore are oriented pointing toward the tip. The amine down conformation is the only conformation that yields results consistent with experiment. The aforementioned results provide a clear indication that this computational method is generally able to reproduce the bright areas in the STM images and can be used to help distinguish between different conformations of a given molecule in STM images.

The calculated plots discussed above illustrate the importance of the interplay between the geometry and electronic structure of the adsorbed molecule. When the functional group points toward the tip, the tip−adsorbate distance is smaller than when the functional group lies in the plane of the carbon backbone. Thus, the tunneling current is expected to increase. However, when the functional group lies in the plane of the carbon backbone, the electronic coupling between the functional group and the surface is expected to be higher, thereby enhancing the tunneling current. The interplay between the electronic structure and molecular geometry is illustrated by performing static charge fitting calculations on both the up and flat orientations of the molecules discussed above. Tables 10−13 show results for the Br and I functionalities for short chain alkanes. In both cases, placing the functional group in the up conformation causes the electronic charge to localize on the functional group. This localization is due to the fact that the functional group is not as strongly coupled to the surface in the up orientation, thereby resulting in a decrease in the ability of the charge on the functional group to redistribute itself on other areas of the adsorbate−surface complex. Thus, both electronic and geometric factors need to be considered in the interpretation of STM images. In the systems studied above, the thiol in the flat conformation provides an example of a system where the electronic coupling of the sulfur atom to the surface is strong enough to yield an enhanced tunneling current in the STM image, even though the sulfur is farther away from the tip than it is in the up orientation. In the cases of the bromine and iodine, however, it is the decreased tip−adsorbate distance in the up orientation that is responsible for the enhanced tunneling current in the vicinity of the functional group.

TABLE 10: Charge Fitting for $CH_3CH_2CH_2CH_2Br$ (up) on One Layer of Graphite

atom	neutral	with added electron
Br	−0.18501	−0.24562
C(1)	−0.40230	−0.30928
H	0.18615	0.18295
H	0.19981	0.17849
C(2)	0.13518	0.12409
H	0.02151	−0.00151
H	−0.01797	−0.00942
C(3)	0.19483	0.23239
H	−0.03285	−0.02996
H	−0.02557	−0.05197
C(4)	−0.34391	−0.34573
H	0.08815	0.08376
H	0.06477	0.04121
H	0.07585	0.09452

TABLE 11: Charge Fitting for $CH_3CH_2CH_2CH_2I$ (up) on One Layer of Graphite

atom	neutral	with added electron
I	−0.47198	−0.56755
C(1)	−0.01250	0.09383
H	0.11842	0.12437
H	0.14315	0.13283
C(2)	−0.00362	−0.05251
H	0.04006	0.03441
H	0.05298	0.06620
C(3)	0.29030	0.34011
H	−0.05037	−0.05465
H	−0.06134	−0.08452
C(4)	−0.32266	−0.33004
H	0.08647	0.08398
H	0.07023	0.04780
H	0.05839	0.08196

TABLE 12: Charge Fitting for $CH_3CH_2CH_2CH_2Br$ (flat) on One Layer of Graphite

atom	neutral	with added electron
Br	−0.16630	−0.18106
C(1)	−0.34256	−0.32680
H	0.16294	0.13683
H	0.17100	0.18602
C(2)	0.07812	0.08843
H	0.02300	−0.00111
H	0.02043	0.03620
C(3)	0.18643	0.20209
H	−0.04593	−0.03635
H	−0.02854	−0.05393
C(4)	−0.31053	−0.30160
H	0.07829	0.07133
H	0.05942	0.03424
H	0.07223	0.08845

TABLE 13: Charge Fitting for $CH_3CH_2CH_2CH_2I$ (flat) on 1 Layer of Graphite

atom	neutral	with added electron
I	−0.09304	−0.10269
C(1)	−0.57427	−0.58552
H	0.20284	0.18580
H	0.24430	0.26837
C(2)	0.20067	0.20810
H	−0.00817	−0.03032
H	−0.01404	0.00619
C(3)	0.23347	0.25595
H	−0.07134	−0.06655
H	−0.03979	−0.06134
C(4)	−0.32641	−0.32805
H	0.08007	0.07562
H	0.05718	0.03708
H	0.07354	0.08720

The degree to which the tunneling current is enhanced depends on the identity of the functional group. The preceding calculations suggest that the degree to which the tunneling current is enhanced in the vicinity of a functional group is directly related to the functional group's polarizability. The more polarizable atoms produce larger changes in the observed tunneling current.

All the preceding plots have been calculated for the transfer of an electron from the tip to the adsorbate−surface complex. Preliminary calculations on halogenated alkanes indicate that there is no significant change in the calculated plots when the electron is transferred from the adsorbate−surface complex to the tip. This finding is consistent with the experimental findings for halogenated alkanes on a graphite surface. Further calculations will involve studying this symmetry on surfaces other than graphite.

VII. Conclusions

The electron-transfer model applied to scanning tunneling microscopy of physisorbed molecules has proven to be of considerable value in interpreting STM images. The method can reproduce the prominent qualitative features of STM images and can be used to distinguish between different conformations for a given molecule. As discussed above, the results indicate that the chlorine and thiol functionalities lie flat in the plane of the carbon backbone, while the bromine and iodine atoms are pointed out of the plane of the backbone toward the tip. The qualitative agreement between the calculated results and the experimental findings indicates that the electron-transfer model provides a reasonable description of the structure of the molecules imaged by the STM.

The deviations of the computational predictions from the experimental data are in part due to the fact that not all experimental factors have been accounted for in the present study. In particular, the presence of additional molecules and of solvent above the adsorbate will affect the STM images. The interaction between molecules within a given layer is certain to have an effect on the STM image of the system. Nevertheless, the calculated images provide crucial information about the experimentally obtained images.

The approach taken in this study has far more general applications. We have shown that one can model certain properties of a bulk solid using only a small cluster of atoms. However, the size of the cluster is extremely important. We have shown that the use of a short-chain adsorbate with a single layer of graphite would have been inadequate to model the tunneling current of adsorbates on graphite. Thus, the first step in designing a cluster model is to ensure that the cluster is chosen such that it does not ignore any important contributions of any other parts of the system. Only after these preliminary steps can the cluster model accurately reproduce the properties of the system of interest.

The versatility of the current method is perhaps the strongest argument for its use. The calculations can be performed for various surfaces and various geometries without requiring any changes to the code. The approach is limited by the necessary CPU time required to calculate the STM images.

Further study will involve reevaluating several of the approximations made in the model. In particular, the band structure of the electrodes will be incorporated into the calculation in order to eliminate many of the approximations made in the use of a cluster model. Similarly, the use of a constant, homogeneous electric field between the tip and sample will be reevaluated, as such a model is not an accurate representation of the field, particularly in the region of the tip. Several other calculations will be performed in order to determine the tunneling current dependence on surface−adsorbate distance, surface−tip distance, and adsorbate−tip distance. The use of new algorithms for the optimization of the adsorbate structures is also being investigated. The combination of faster and more accurate algorithms will lead to a more complete understanding of the processes involved in scanning tunneling microscopy.

Acknowledgment. Special thanks are due to Dr. Leanna Giancarlo and all the members of the Flynn group for their encouragement and many useful discussions and to Noah Z. Burns for his help in making the figures. This research was supported in part by grants from the Department of Energy (DE-FG02−90ER14162) to R.A.F. and grants to G.W.F. from the National Science Foundation (CHE-00−95649) and in part by the Columbia Materials Research Science and Engineering Center (DMR-98−09687).

References and Notes

(1) Tersoff, J.; Hamman, D. R. *Phys. Rev. Lett.* **1983**, *50*, 1998.
(2) Tersoff, J.; Hamman, D. R. *Phys. Rev. B.* **1985**, *31*, 805.
(3) Eigler, D. M.; Weiss, P. S.; Schweizer, E. K.; Lang, N. D. *Phys. Rev. Lett.* **1991**, *66*, 1189.
(4) Ou-Yang, H.; Kallebring, B.; Marcus, R. A. *J. Chem. Phys.* **1993**, *98*, 7565.
(5) Magonov, S. N.; Whangbo, M.-H. *Adv. Mater.* **1994**, *6*, 355.
(6) Dabrowski, J.; Mussig, H.-J.; Wolff, G. *Phys. Rev. Lett.* **1994**, *73*, 1660.
(7) Faglioni, F.; Claypool, C. L.; Lewis, N. S.; Goddard, W. A., III *J. Phys. Chem. B* **1997**, *101*, 5996.
(8) Corbel, S.; Cerda, J.; Sautet, P. *Phys. Rev. B* **1999**, *60*, 1989.
(9) Coley, T. R.; Goddard, W. A., III.; Baldeschwieler, J. D. *J. Vac. Sci. Technol. B* **1991**, *9*, 470.
(10) Zhang, L. Y.; Friesner, R.; Murphy, R. B. *J. Chem. Phys.* **1997**, *107*, 450.
(11) Hay, P. J.; Wadt, W. R. *J. Chem. Phys.* **1985**, *82*, 270.
(12) Hay, P. J.; Wadt, W. R. *J. Chem. Phys.* **1985**, *82*, 284.
(13) JAGUAR v.3.5, Schrodinger, Inc., Portland, OR, 1998.
(14) Friesner, R. A. *Chem. Phys. Lett.* **1985**, *116*, 39.
(15) Friesner, R. A. *J. Chem. Phys.* **1987**, *86*, 3522.
(16) Ringnalda, M. N.; Belhadj, M.; Friesner, R. A. *J. Chem. Phys.* **1990**, *93*, 3397.
(17) Greeley, B. H.; Russo, T. V.; Mainz, D. T.; Friesner, R. A.; Langlois, J.; Goddard, W. A., III.; Donnelly, R. E.; Ringnalda, M. N. *J. Chem. Phys.* **1994**, *101*, 4028.
(18) Sautet, P.; Dunphy, J. C.; Ogletree, D. F.; Joachim, C.; Salmeron, M. *Surf. Sci.* **1994**, *315*, 127.
(19) Cyr, D. M.; Venkataraman, B.; Flynn, G. W.; Black, A.; Whitesides, G. W. *J. Phys. Chem.* **1996**, *100*, 13747.
(20) Claypool, C. L.; Faglioni, F.; Matzger, A. J.; Goddard, W. A., III; Lewis, N. S. *J. Phys. Chem. B* **1999**, *103*, 9690.
(21) Claypool, C. L.; Faglioni, F.; Goddard, W. A., III; Gray, H. B.; Lewis, N. S.; Marcus, R. A. *J. Phys. Chem. B* **1997**, *101*, 5978.
(22) Mujica, V.; Kemp, M.; Ratner, M. A. *J. Chem. Phys.* **1994**, *101*, 6856.